

Space Weather

RESEARCH ARTICLE

10.1029/2018SW001866

Special Section:

Space Weather Events of 4–10
September 2017

Key Points:

- The largest outburst, in frequency and magnitude, of Solar Cycle 24 occurred late in the cycle from 4 to 10 September 2017
- These solar flares were well observed in the EUV by SDO EVE and other solar EUV irradiance instruments and modeled by FISM
- The 6 and 10 September X-class flares are remarkably similar in physical evolution and irradiance spectral evolution

Supporting Information:

- Movie S1
- Movie S2

Correspondence to:

P. C. Chamberlin,
phil.chamberlin@lasp.colorado.edu

Citation:

Chamberlin, P. C., Woods, T. N., Didkovsky, L., Eparvier, F. G., Jones, A. R., Machol, J. L., et al. (2018). Solar ultraviolet irradiance observations of the solar flares during the intense September 2017 storm period. *Space Weather*, 16, 1470–1487. <https://doi.org/10.1029/2018SW001866>





Received 15 MAR 2018

Accepted 17 AUG 2018

Accepted article online 31 AUG 2018

Published online 2 OCT 2018

Solar Ultraviolet Irradiance Observations of the Solar Flares During the Intense September 2017 Storm Period

P. C. Chamberlin¹ , T. N. Woods¹ , L. Didkovsky², F. G. Eparvier¹ , A. R. Jones¹, J. L. Machol^{4,5}, J. P. Mason³, M. Snow¹, E. M. B. Thiemann¹ , R. A. Viereck⁴, and D. L. Woodraska¹

¹Laboratory for Atmospheric and Space Physics, University of Colorado Boulder, Boulder, CO, USA, ²Space Science Center, University of Southern California, Los Angeles, CA, USA, ³Solar Physics Laboratory, NASA Goddard Space Flight Center, Greenbelt, MD, USA, ⁴Space Weather Prediction Center, NOAA, Boulder, CO, USA, ⁵Cooperative Institute for Research in Environmental Sciences, University of Colorado Boulder, Boulder, CO, USA

Abstract A large outburst of flares occurred between 4–10 September 2017 when new magnetic flux emerged into and strengthened an existing active region, National Oceanic and Atmospheric Administration Region 12673. This intense solar storm period included X9.3 (6 September) and X8.2 (10 September) flares, the largest flares that have occurred during Solar Cycle 24, as well as 39 M-class flares and three additional X-class flares. Another X-class flare from this active region was observed on the farside of the Sun from Mars Atmosphere and Volatile Evolution prior to the September events, along with other large M-class flares, showing the potential for how farside irradiance monitoring can improve flare prediction at Earth for 1- to 13-day forecasts. This September 2017 flare period is similar to other famous storm periods such as the 18 October to 5 November 2003 Halloween storm that produced 14 X-class flares and 137 M-class flares and the 6–10 September 2005 period that had 11 X-class and 68 M-class flares. All of these storm periods occurred in the declining phase of the solar cycle when solar activity had decreased significantly from solar maximum levels. This paper focuses on a number of solar irradiance observations at ultraviolet (0–190 nm) wavelengths during the September 2017 storm period and the advantages that an ensemble of measurements and models have for studying solar flares.

1. Introduction

Observations of the solar irradiance are used to quantify the variable energy output of the Sun and subsequently used to estimate changes in Earth and other planetary atmospheres where this energy is deposited. Historically, space-based irradiance instruments have been used to observe variations in intensity over the 11-year solar cycle and 27-day solar rotation period, only requiring observations of approximately daily cadence over many years. More recently, instruments have optimized signal levels, cadence, and duty cycle to study variations due to solar flares that can significantly change irradiance values on timescales of seconds to hours. While most of the science goals of these irradiance instruments are still to accurately measure and quantify the changing energy input into planetary systems, these observations have also proven valuable to the solar physics community due to their large spectral coverage in ultraviolet (UV) wavelengths and nearly continuous and rapid observation cadence. The long-standing monitor for solar flares for space weather operations has been the X-Ray Sensor (XRS) aboard a series of Geostationary Operational Environmental Satellites (GOES) since the 1970s. Since then, a much larger suite of solar irradiance instruments that have been launched are providing much more details about solar flares themselves and the influence they have on planetary bodies.

A number of solar irradiance observatories were available to provide valuable data sets for storm periods prior to the September 2017 flares, although not all of these instruments were optimized to study these events because of reduced temporal cadence and duty cycle. Regardless, valuable studies looking at the evolution and energetics of solar flares as well as their space weather impact on planetary systems have been performed using these data. Chamberlin et al. (2008) used 27 flares observed with Solar EUV Experiment (SEE) to produce an empirical model, called the *Flare Irradiance Spectral Model* (FISM) to estimate the solar irradiance from 0.1 to 190 nm at 1-min cadence to quantify the solar spectral enhancement across the entire wavelength range due to solar flares. These SEE-based FISM results have been primarily used in numerous studies to quantify the ionospheric and thermospheric (I/T) responses to the increased UV irradiance

during solar flares (Peterson et al., 2008; Qian et al., 2010; Qian et al., 2011; Qian, Burns, Liu, et al., 2012; Qian, Burns, Solomon, et al., 2012). Using FISM, Lolo et al. (2012) modeled the response of the ionosphere of Mars to a solar flare and Sternovsky et al. (2008) quantified the variability of the lunar photoelectron sheath to solar flares. These studies indicate an almost instant response in the ionosphere and heating of the thermosphere proportional to the solar irradiance increase. Woods et al. (2006) and Moore et al. (2014) were able to use measurements of a few large flares observed by the Solar Radiation and Climate Experiment (SORCE; Rottman, 2005) Total Irradiance Monitor (TIM; Kopp et al., 2005), as well as Thermosphere, Ionosphere, Mesosphere, Energetics, and Dynamics (TIMED) SEE, GOES XRS, and FISM results of during the October/November 2003 and September 2005 storm periods to quantify the total radiative loss that occurred in solar flares, to differentiate between the energy loss in the impulsive and gradual phases, and to model the total radiative energy loss for other flares. With the new suite of instruments, many of them optimized for high-cadence flare observations, that were available to concurrently observe the September 2017 flare events, much greater accuracy and details of large solar flares, and their impact on planetary atmospheres will be achieved.

The goals of this paper are to provide a brief overview of the many irradiance observations and model results that are available during the September 2017 storm period. Section 1 presents a summary of the flares that occurred during this storm period, followed by section 3 that gives an instrument summary and subset of the substantial solar irradiance observational data and empirical modeling results available from the September 2017 storms. Section 4 concludes with a summary of the presented results and comparisons.

2. Instruments Observing and Model Results of the September 2017 Storm Period

The September 2017 storm period occurred while a large number of complimentary irradiance instruments were contemporaneously operational. These instruments, described in detail in this section, span multiple platforms in the Heliophysics Great Observatory including TIMED and Solar Dynamics Observatory (SDO), as well as the Mars Atmosphere and Volatile Evolution Mission's (MAVEN) Extreme Ultraviolet Monitor (EUVM) instrument from the NASA planetary division and the National Oceanic and Atmospheric Administration's GOES mission.

2.1. GOES EXIS

The GOES XRS (Garcia, 1994), with measurements in two soft X-ray bands from 0.1 to 0.8 nm and 0.05 to 0.4 nm, is optimized for flare observations and can be used to identify the start, peak, and end times of a flare and is the definitive instrument to classify the magnitude of solar flares. This solar flare classification uses the GOES XRS-B (0.1–0.8 nm) magnitude, which then is translated by decade into a flare index classification ranging from A- to X-class flares. A-class flares start at $1 \times 10^{-8} \text{ W/m}^2$, and the B-, C-, M-, and X-class flares start at a factor of 10 more than the previous class. There is also the XRS-A (0.05–0.4 nm) band that is used with XRS-B for space weather operations to predict when a flare peak will occur for science analysis to estimate the coronal plasma temperature and emission measure (density).

The new, updated GOES-16 XRS (Chamberlin et al., 2009) is now part of a larger instrument suite known as the EUV and X-ray Irradiance Sensors (EXIS) that includes a new instrument with many wavelengths extending into the UV called the EUV Sensor (EUVS; Eparvier et al., 2009). To cover the large dynamic range (greater than 5 orders of magnitude) of the solar X-ray variability, the new GOES-16 and beyond (GOES-R series) versions of the XRS have split the range into two channels for each wavelength band. The quiet sun channels, "A1" and "B1," have a large aperture while the solar flare "A2" and "B2" channels have a smaller aperture. The 1 and 2 channels for both wavelength ranges overlap in magnitude coverage.

The three EUVS channels are EUVS-A that measures 25.6 nm (He II during quiet Sun conditions, dominated by Fe XXIV during flares), 28.4 nm (Fe XV), and 30.4 nm (He II), EUVS-B that measures 117.5 (C III), 121.6 nm (H I), 133.5 nm (C II), and 140.5 nm (Si IV/O IV blend), and EUVS-C that measures the solar spectra near 280 nm to produce the Mg II index (Snow et al., 2009). The GOES-16 XRS and EUVS solar observations have cadence of 1 and 30 s, respectively. GOES-16 EUVS measurements do exist for this September 2017 flare period but have not yet been made public so are not included here.

2.2. SDO EVE

The EUV Variability Experiment (EVE; Woods et al., 2012) was launched aboard the SDO (Pesnell et al., 2012) in 2010 and is the follow-on to TIMED SEE. SDO EVE was designed to measure the solar spectrum from 6 to 106 nm at 0.1-nm resolution every 10 s using the Multiple EUV Grating Spectrograph (MEGS) A and B channels, which span the 6- to 37- and 33- to 106-nm ranges, respectively. SDO is in geosynchronous orbit, like GOES; so EVE observations are nearly continuous with only occasional eclipse periods. MEGS-A was lost on 26 May 2014 due to a CCD power supply capacitor failure, so unfortunately, no MEGS-A data are available for the September 2017 storm period. MEGS-B was discovered to have an accelerated degradation profile shortly after launch, so it has been limited to approximately 3-hr observing windows each day. Recently, the on-board operational software for MEGS-B was updated to trigger a flare campaign mode that puts MEGS-B in science mode for 3 hr if a flare reaches an M1 level or higher. This flare mode will restart, and continually trigger, each time an M-class flare has been reached regardless of whether it is still in flare mode from a previous flare, and there is no limit to the number of flare campaigns that can be triggered. This MEGS-B mode of operation was especially advantageous during this September 2017 period, when there ended up being nearly 75% coverage during the 8 days of this flare period instead of the standard 12% coverage during no flare campaigns.

The fourth instrument of EVE, the EUV SpectroPhotometer (ESP; Didkovsky et al., 2012), is a set of broadband photodiode channels in the soft X-ray wavelength range with 0.25-s cadence. The central order channel covers the 0.1- to 7-nm range, while the first-order channels are centered on 18.2, 25.7, 30.4, and 36.6 nm, all with approximately 6-nm-wide spectral band-passes. ESP still operates at nearly 100% duty cycle, although SDO experiences short eclipses (<70 min/day) during September.

There have already been a large number of studies of flares prior to this September 2017 storm period with the EVE instrument, with many significant findings including a new flare “late phase” (Woods et al., 2011), more accurate quantification of the energetics and thermal evolution during flares (Chamberlin et al., 2012; Milligan et al., 2014; Ryan et al., 2013), as well as studies of Doppler shifts of plasma dynamics (flow) during solar flares (Chamberlin, 2016; Hudson et al., 2011). These studies, along with the I/T studies discussed in section 2.2, should be performed for the September 2017 flares given these were the largest flares observed by EVE and of Solar Cycle 24.

2.3. SDO AIA

SDO also has a multichannel UV imager, the Atmospheric Imaging Assembly (AIA; Lemen et al., 2012). The high-cadence and full-disk, high spatial resolution images from AIA provide invaluable information as to the plasma dynamics of the loops and footpoints during the flare events and context for the source of the EUV irradiance variations observed by EVE. SDO AIA was fully functional in its normal observing mode during these flares and has provided detailed images and movies of the events.

2.4. TIMED SEE

The SEE instrument on the TIMED satellite became operational in early 2002 and is still currently operating. SEE comprises two instruments, the EUV Grating Spectrograph (EGS; Woods et al., 2005) that measures from 27 to 190 nm with 0.4-nm resolution, and the X-ray Photometer System (XPS; Woods & Rottman, 2005) that consists of a set of broadband diodes, where only the one channel from 0 to 7 nm still works following a filter mechanism failure on 24 July 2002. A SEE Level 4 data product uses the CHIANTI solar model (Del Zanna et al., 2015; Dere et al., 1997; Landi et al., 2013), driven by the XPS measurements, estimates the spectral distribution in the 0- to 40-nm range, at better than 0.1-nm spectral resolution (Woods et al., 2008). The SEE Level 3 product combines the XPS model spectra from below 27 nm and the EGS spectra above 27 nm into 1-nm intervals.

SEE was designed to produce an accurate daily-average solar irradiance product. With its 1-axis solar pointing platform, SEE takes a series of 10-s integrations in a single 3-min observing window for each orbit, whose period is approximately 96 min. Chamberlin et al. (2008) applied instrument corrections to each individual 10-s integration in order to use these higher, 10-s cadence observations to study flares, but this is more critical for the rapidly changing impulsive phase. Since the SEE observations for the flares presented here were during the gradual phase of long-duration flares, not much variation is expected over the observations, so the standard, publicly available Level 2 product is used that is the full 3-min integration.

2.5. MAVEN EUVM

The MAVEN EUVM (Eparvier et al., 2015) measurements are similar in nature to the XPS measurements, in that the EUVM band-pass filters and Si photodiode response define the extent of the broad wavelength coverage for the different EUVM channels. EUVM has three channels: 17–22 nm (Channel A), 0.1–7 nm (Channel B), and a hydrogen Lyman-alpha channel centered at 121.6 nm (Channel C). The measurements of the solar irradiance at Mars from these three EUVM diodes are used as proxies to produce the FISM for Mars (FISM-M; Thiemann et al., 2017). Estimates from FISM-M of the full UV solar spectral irradiance from 0 to 190 nm are input into the Martian atmosphere as the official EUVM Level 3 product.

2.6. FISM

Version 2 of the FISM is nearly released, and initial estimations from FISM2 of the solar irradiance from 0.1 to 190 nm during this storm period are available at 1-min cadence and 0.1-nm bins, an improvement from the 1.0-nm bins of FISM version 1 (Chamberlin et al., 2007, 2008). FISM2 is based on SORCE SOLSTICE XPS Level 4, Version 11 data (Woods et al., 2008), the Miniature X-ray Solar Spectrometer (MinXSS; Mason et al., 2016; Woods et al., 2017), SDO EVE MEGS A/B Level 3, version 6 (Woods et al., 2012), and SORCE SOLSTICE version 18, high-resolution (McClintock et al., 2005) data products. These data provide the necessary 0.1-nm spectral resolution at high temporal cadence and have included a significant amount of flare observations, which leads to a significant improvement in accuracy over FISM1 whose flare component was based solely on TIMED SEE at 1.0-nm resolution and only 27 flares. The FISM2 cadence will be increased to 10 s in the future.

3. Flare Observations and Models for September 2017 Flares

The September 2017 flare period began with the emergence of new active region flux from below the surface into an existing active region. The previously existing active region had produced one X-class and two large M-class solar flares on the farside of the Sun as observed from the MAVEN's (Jakosky et al., 2015) Solar EUVM (Eparvier et al., 2015) instrument in July, which could have provided a valuable data set for long-term space weather predictions if a similar instrument was operated with the more complex real-time operational mode. Although it had decayed to a less magnetically complex bipolar active region by early September, the emergence of this new group of flux through the surface just prior to the storm period caused the entire active region to become more magnetically complex and enhanced the opportunity for reconnection events and solar eruptions to occur (Yang et al., 2017).

A summary table of the M-class and larger flares for the period from July through September 2017 is given in Table 1. This shows information on the timing, magnitude, and instruments that observed each event. There are also columns showing, which flare events had strong impulsive phases, coronal dimming, or associated CMEs. A sample of the measurements and results from these instruments described in section 2 are presented here, as well as the results from the FISM empirical model.

3.1. SDO AIA Measurements

Summary movies created using Helioviewer.org of all AIA wavelengths can be found in the supporting information. AIA images shown in Figures 1 and 2 highlight various events in the two large flares, the X9.3 flare on 6 September and the X8.2 flare on 10 September, respectively. Each of the subpanels, (a)–(i), correspond with various events seen in the SDO/EVE time series presented in Figure 4 to provide insight on the source and the dynamics of the EUV irradiance variations.

The AIA images show a complex and extended evolution, with at least three distinct sections of reconnecting arcades along the entire flare arcade. Both flares have an initial, quick reconnection in the center of the arcade seen in Figures 1b and 2b for the two events. The reconnection then continues further down to the south in the arcade seen in Figures 1c and 2c. A third distinct reconnecting and continuing of the arcade expansion can be seen going out to the top of the images in Figures 1d/f and 2e. The extensions of the arcade both up and down as seen in the images are much slower to advance but eventually make for a very large and curved arcade of postflare loops seen in Figures 1g–1h and 2g–2h—a very similar evolution for both the 6 and 10 September flares. For the 10 September flare, no visible evidence of low-atmosphere footpoints or ribbons are noticeable until around 16:05 when a ribbon from the southern arcade reconnection expansion becomes visible on the limb and extends onto the surface visible from Earth and AIA.

Table 1
Detailed Information on Each Flare of M-Class or Above During the September 2017 Storm Period

GOES Flare	Date	Start time	Peak	End time	Location	AR number	Flare observations				STEREO or SOHO CME		
							SDO	TIMED SEE	SORCE	MAVEN		GOES-16	Impulsive phase ESP
M1.3	7/3/17	1537	1615	1618			ESP only	No	No	Yes	Yes	Yes	LASCO
M1.3	7/9/17	0309	0318	0337	S08E37	2665	ESP + MB	No	Decline	No	Yes	No	No
M2.4	7/14/17	0107	0209	0324	S06W29	2665	ESP + MB	Rise	Rise, Decline	No	Yes	No	No
X2.8	7/23/17	0420	0505	1500	Farside		No	No	No	Yes	Yes (Lya)	No	LASCO
M7.9	7/28/17	0250	0315	0500	Farside		No	No	No	Yes	Yes (Lya)	No	LASCO
M5	7/28/17	0500	0505	1100	Farside		No	No	No	Yes	Yes (Lya)	No	LASCO
M1.1	8/20/17	0136	0152	0203	N05E84	2672	ESP only	No	Peak (& rise)	Decline	Maybe	Maybe	No
M1.2	9/4/17	0536	0549	0605	S10W04	2673	ESP only	No	Decline	No	No	No	No
M1.5	9/4/17	1511	1530	1533	S06W13	2673	ESP only	No	No	No	Yes	No	No
M1.0	9/4/17	1805	1822	1831	S12W60	2673	ESP only	No	No	No	Yes	Maybe	LASCO
M1.7	9/4/17	1846	1937	1952		2673	ESP only	No	No	No	Yes	No	Might be prior
M1.5	9/4/17	1959	2002	2006		2673	ESP only	No	No	No	Yes	No	LASCO
M5.5	9/4/17	2028	2033	2037		2673	ESP + MB	No	Peak	No	Yes	No	Might be prior
M2.1	9/4/17	2210	2214	2219	S06W15	2673	ESP + MB	No	Peak	No	Yes	No	LASCO
M4.2	9/5/17	0103	0108	0111	S11W16	2673	ESP + MB	No	No	No	Yes	Yes	LASCO
M1.0	9/5/17	0342	0351	0404		2673	ESP + MB	No	No	No	Yes	No	No
M3.2	9/5/17	0433	0453	0507		2673	ESP + MB	No	No	No	Yes	No	No
M3.8	9/5/17	0633	0640	0643		2673	No	No	Peak (& rise)	No	No	No	LASCO
M2.3	9/5/17	1737	1743	1751	S09W24	2673	ESP + MB	No	Peak	No	Yes	No	No
X2.2	9/6/17	0857	0910	0917	S08W33	2673	No	No	Decline	No	Yes	No	LASCO
X9.3	9/6/17	1153	1202	1210		2673	ESP + MB	No	Decline	No	Yes	Yes	LASCO
M2.5	9/6/17	1551	1556	1603	S09W38	2673	ESP + MB	No	Decline	No	Yes	No	LASCO
M1.4	9/6/17	1921	1930	1935	S07W44	2673	ESP only	No	No	No	Yes	No	No
M1.2	9/6/17	2333	2339	2344		2673	ESP only	No	Peak (weak)	No	Yes	No	No
M2.4	9/7/17	0459	0502	0508	S07W45	2673	ESP only	No	Decline	No	Yes	No	No
M1.4	9/7/17	0949	0954	0958	S08W47	2673	ESP only	No	Peak (weak)	Yes (OTL)	Yes	Yes	No
M7.3	9/7/17	1011	1015	1018		2673	ESP only	No	No	No	Yes	No	LASCO
X1.3	9/7/17	1420	1436	1455	S11W49	2673	ESP + MB	No	Decline	Yes (OTL)	Yes	Yes	Might be prior
M3.9	9/7/17	2350	2359	0014	S06W53	2673	ESP + MB	No	Decline	No	Yes	No	LASCO
M1.3	9/8/17	0219	0224	0229	S07W55	2673	ESP + MB	No	Decline	No	Yes	Maybe	No
M1.2	9/8/17	0339	0343	0345	S06W55	2673	ESP + MB	No	No	No	Yes	No	No
M8.1	9/8/17	0740	0749	0758	S10W57	2673	No	Rise	No	No	Yes	No	LASCO
M2.9	9/8/17	1509	1547	1604	S08W68	2673	ESP + MB	No	Decline	Decline	Yes	No	STEREO-A
M2.1	9/8/17	2333	2345	2356		2673	ESP + MB	Peak/Decline	Decline	Yes (OTL)	Yes	No	No
M1.1	9/9/17	0414	0428	0443	S13W69	2673	ESP + MB	Peak	No	Yes (OTL)	Yes	No	No
M3.7	9/9/17	1050	1104	1142	S14W74	2673	ESP + MB	Peak	No	Yes (OTL)	Yes	No	No
M1.1	9/9/17	2204	2353	0041		2673	ESP only	No	Decline	Decline	Yes	No	LASCO
X8.2	9/10/17	1535	1606	1631		2673	ESP + MB	Peak/Decline	Decline	Yes	Yes	Yes	LASCO
M3.4	9/17/17	1145	2100	2100	Farside		No	No	No	Yes	Yes (Lya)	Yes	4 CMEs in this

Note. Included are flares observed by MAVEN/EUVI from the same active region location, where timings given for MAVEN events is time as observed at Mars. Also provided are the NOAA active region number and times, available instrument measurements, and if the flare had an associated impulsive phase, coronal dimming, and/or associated CME. The red shading highlights the X-class flares that were observed on Earth. NOAA = National Oceanic and Atmospheric Administration; MAVEN = Mars Atmosphere and Volatile Evolution; EUVM-B = Extreme Ultraviolet Monitor-B; STEREO = Solar Terrestrial Relations Observatory; SOHO = Solar and Heliospheric Observatory; GOES = Geostationary Operational Environmental Satellite; AR = Active Region; SDO = Solar Dynamics Observatory; TIMED SEE = Thermosphere, Mesosphere, Energetics, and Dynamics Solar EUV Experiment; SORCE = Solar Radiation and Climate Experiment; ESP = EUV SpectroPhotometer; CME = coronal mass ejection; LASCO = Large Angle and Spectrometric Coronagraph.

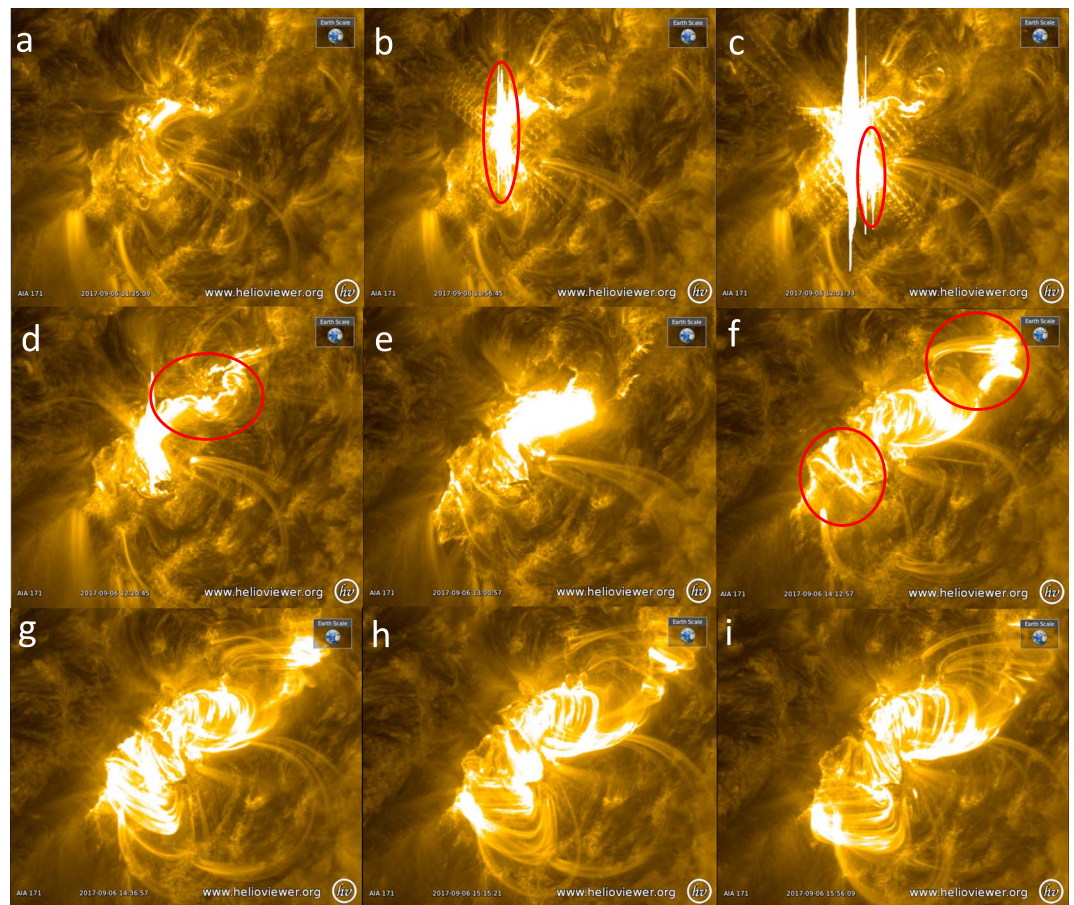


Figure 1. SDO AIA 17.1-nm image sequence during the X9.3 flare on 6 September 2017. Red circles show the location of new postflare loops and are associated with new peaks in the SDO EVE time series. These new postflare loops indicate new regions of reconnection or temporally disconnected regions along the flare arcade that are delayed from the initial, centrally located eruption. Each panel shown is from the same time as a significant event or new peak in the SDO EVE time series in Figures 4a and 4c to allow for direct comparisons between the source in the images and the enhanced irradiance emissions as seen by EVE. AIA = Atmospheric Imaging Assembly; SDO = Solar Dynamics Observatory; EVE = EUV Variability Experiment.

3.2. SDO EVE Measurements

Figure 3 shows the complete time series during the September 2017 storms for the SDO/EVE/ESP 0–7 nm channel (a), the SDO/EVE/MEGS-B 56.78 nm Fe XX line using the EVE Version 6, Level 2 Line data product (b), and the MAVEN/EUVM-B 0–7 nm observations (c; MAVEN/EUVM measurements are described in section 3.4). ESP still has an almost 100% duty cycle, where the small gaps in these data are due to eclipses. The MEGS-B data can be sparse but are more frequent than usual as the “flare-campaign” mode was triggered multiple times during these events, showing the value of this operation mode. The ESP 0–7 nm channel has been shown to compare well with the GOES XRS channels (Hock et al., 2013), with the ESP flare peaks occurring slightly later and broader due to the ESP extended band-pass to longer, cooler wavelengths. The gradual, thermal phases of the two large flares are of comparable magnitude for any hot, coronal emissions. This is expected due to their similar GOES XRS classifications and because the gradual phase is driven mostly by the hot plasma emitted in the upper coronal loops after the flare impulsive phase.

The solar flare that occurred on 6 September was near the center of the disk, so there should not be any center-to-limb variations of the flare occurring that would suppress optically thick emissions due to the high densities of the overlying plasma (Chamberlin et al., 2008; Thiemann et al., 2018). In contrast, the 10 September flare was an “over the limb” event, as seen in the AIA images. The over-the-limb flare means that the Sun has rotated to the point that the active region itself, as well as the footpoints of the flare, have rotated

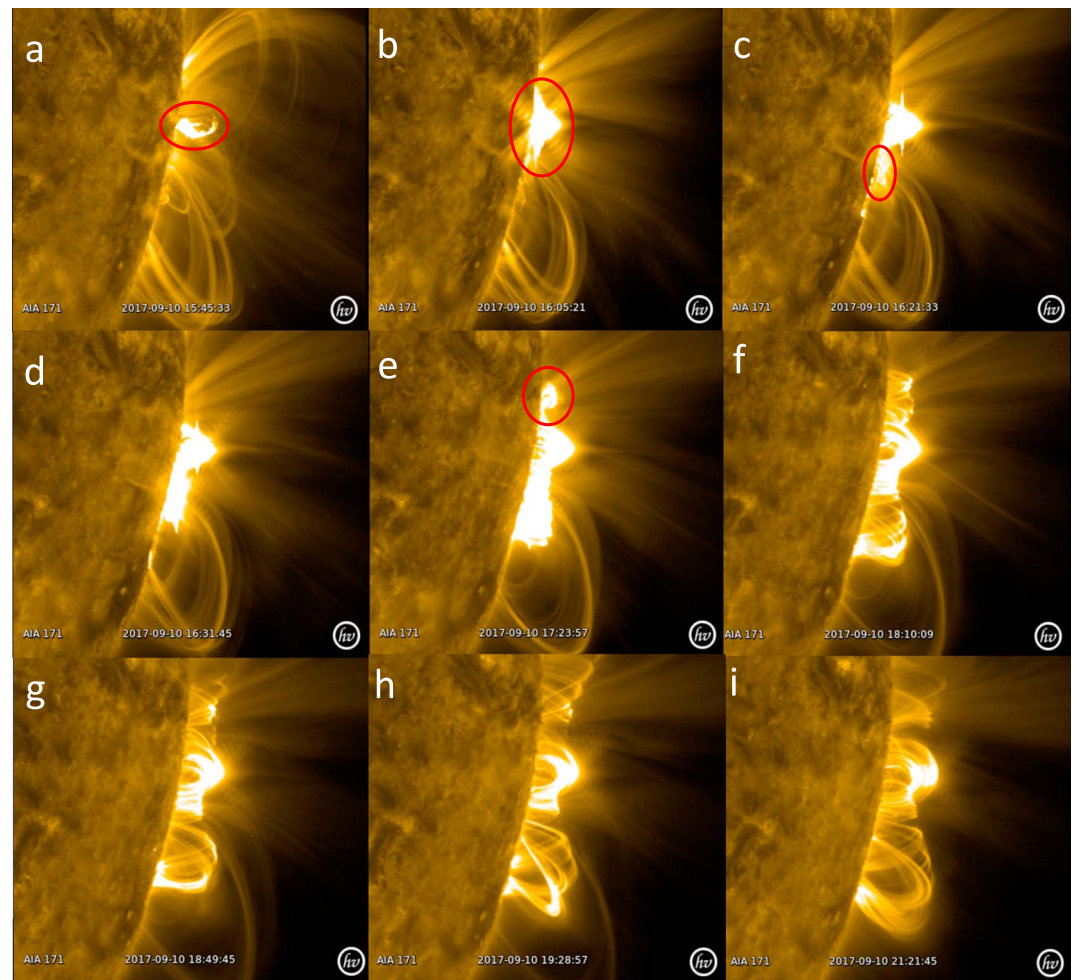


Figure 2. SDO AIA 17.1-nm image sequence during the X8.2 flare on 10 September 2017. As in Figure 1, red circles show the location of the appearance of new postflare loops. Images for this date can be compared with the SDO EVE time series that are given in Figures 4b and 4d. AIA = Atmospheric Imaging Assembly; SDO = Solar Dynamics Observatory; EVE = EUV Variability Experiment.

around to the backside of the Sun as viewed from Earth and are no longer visible. But, the flare loops extend up into the corona are still visible over the limb from Earth. Even though the instruments described in this paper are “irradiance” instruments with no spatial resolution, over-the-limb flares provide unique observations that isolate the emissions that come only from the flaring loops and do not include emissions from the footpoints.

Time series for the 6 September flare and 10 September flare from SDO EVE are shown in Figure 4 for the cooler chromospheric emissions (He I and He II) as well as coronal emissions (0–7 nm, Fe XX, and Fe XVI). The top panels are from the ESP channel while the bottom panels are from the MEGS-B channel. The MEGS-B time series, with good spectral resolution, clearly shows multiple eruptions for both the 6 and 10 September flares, which was not clear using the broadband ESP or the GOES XRS data that span a much broad temperature range than the isolated emission lines observed by MEGS-B. The He I time series shows at least two very distinct impulsive phase enhancements, while the coronal Fe XX and Fe XVI shows the thermal (gradual) phase response of the hot plasma that also shows multiple enhancements throughout the flare. These can be correlated in time, as labeled at the top of Figure 4, with the AIA images and panels labeled (a)–(i) in Figures 1 and 2 that shows at least three different parts of the flare arcade enhancing at different times. There is approximately three times smaller emission for the chromospheric He II emission line (panel (b)) and an order of magnitude smaller He I (panel (d)) emissions in the 10 September flare due to the occultation of

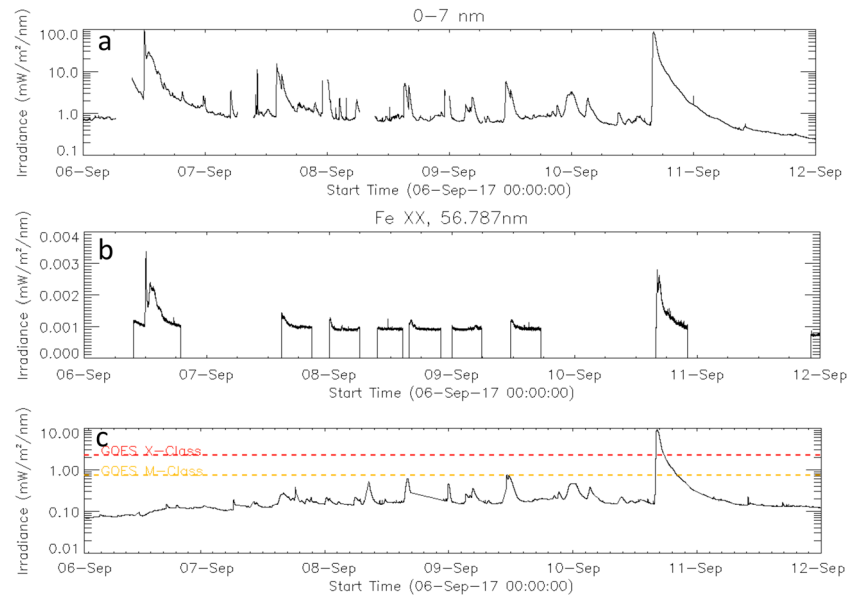


Figure 3. Time series of the SDO/EVE/ESP 0- to 7-nm soft X-ray emission (a), the SDO/EVE/MEGS-B Fe XX 56.78-nm line (b), and the MAVEN/EUVM/Channel-B 0-7 nm (c) during the 6–12 September 2017 storm period. Panel (b) shows the SDO MEGS-B measurements that include many flare campaigns beyond the usual 3-hr/day of observation time. The MAVEN/EUVM measurements show that the early flares were not observed from MAVEN at Mars until the active region rotated around to its view on 8 September. MAVEN had a complete view of the 10 September flare that had its footpoints occulted by Earth-observing observatories. SDO = Solar Dynamics Observatory; EVE = EUV Variability Experiment; EUV SpectroPhotometer; MEGS = Multiple EUV Grating Spectrograph; MAVEN = Mars Atmosphere and Volatile Evolution; EUVM = Extreme Ultraviolet Monitor.

the footpoints that are over the limb as viewed from Earth, so the impulsive phase emission that dominates these cool emissions is eliminated. The timing of the He II peak is delayed as it from the thermal plasma as it cools to the contribution temperatures late in the gradual phase after the soft X-ray and hot coronal emissions peak. Also, it can be seen in the AIA movies that a chromospheric flare ribbon does end up extending over the limb to the side visible from Earth around 16:05 UT, and this is also a source of the He II contributions seen rising after 16:00 UT in Figures 4b and 4d.

The similarities of the two flares are interesting in that not only did both the 6 and 10 September flares have multiple, distinct energy releases, but also that the first energy release was faster and heated the plasma to hotter temperatures, as can be seen by the Fe XX irradiance being relatively higher than the Fe XVI, while in the second energy release, the plasma response is slower, longer, but also the cooler Fe XVI is relatively larger than the hotter Fe XX, meaning the flare plasma temperature did not reach as high with the second energy release in each event. Using the AIA images for context, it can be seen in both flares that the hotter, initial energy release was in the center of the arcade, seen as the red circle in Figures 1b and 2a. The slower, cooler energy releases later in the events are from the enhancements at the ends of the arcade and can first be seen in Figures 1d and 1f and 2c and 2e. The 6 and 10 September flares were not only of similar GOES class, but given the AIA movies and EVE spectral evolution time series, it can be hypothesized that the two flares also have very similar physical arcade evolution, with one viewed from above and one viewed in profile. This opens up the opportunity to study the flare large-scale dynamics (flows) from two viewpoints, while recognizing that smaller scale effects are likely different for these two similar flares.

The complete spectra at all times during each flare can also be shown, given that the MEGS-B channel was functioning during the duration of these flares. The measured MEGS-B spectrum for the 6 September 2017 flare at the peak of the impulsive phase is shown as the black spectrum in Figure 5a, while the daily average spectrum is in red. The impulsive phase spectrum is a 30-s integration centered at 11:57:27 UT, the time of the peak of the He I 53.70 nm emission line as measured by MEGS-B and seen as red in Figure 4c. The absolute magnitude changes in the impulsive phase peak spectrum above the daily average spectrum are shown in Figure 5b. This figure shows the large changes in the chromosphere and transition region emissions that

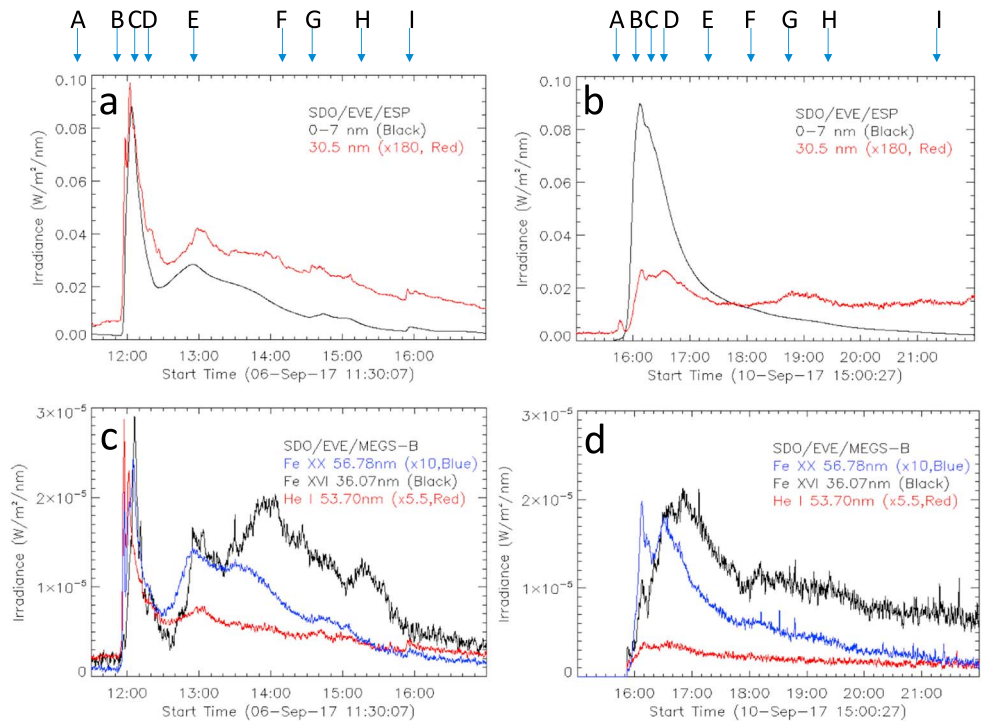


Figure 4. Time series of the flare on 6 September 2017 (a and c) and 10 September 2017 (b and d). Panels (a) and (b) compare the EVE/ESP 0–7 nm (black) and ESP 30.4 nm (red) channels, while panels (c) and (d) compare two observations from EVE/MEGS-B, the hot Fe XX 56.78 and Fe XVI 36.07 nm emissions formed around $\log(T) = 6.9$ (blue) and 6.4 (black), respectively, and the cool He I 53.70-nm emission line formed in the chromosphere at $\log(T) = 3.8$. The 30.4-nm data are scaled by a factor of 180 in panels (a) and (b). The labels A–I at the top of the figure indicate the times of the respective panels (a)–(i) of AIA images in Figure 1 for the 6 September flare and Figure 2 for the 10 September flare. EVE = EUV Variability Experiment; MEGS = Multiple EUV Grating Spectrograph; ESP = EUV SpectroPhotometer.

dominate this wavelength range, including strong bound-bound emission lines as well as the free-bound continua (Milligan et al., 2012).

A similar set of plots as found in Figure 5 can be made for the gradual phase peak for the 6 September 2017 flare. The gradual phase peak spectrum defined by the 30-s integration around the peak of the Fe XX 56.78 nm emission line measured by MEGS-B that occurred at 12:16:16 UT. This is between the “c” and “d”

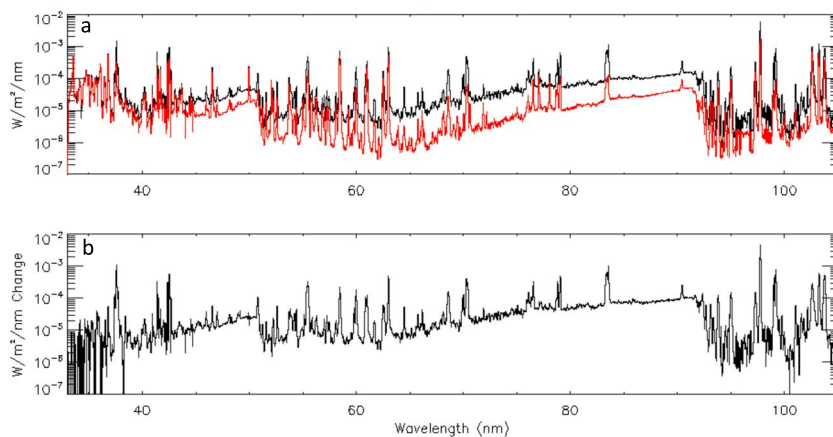


Figure 5. Flare increases for the 6 September 2017 flare during the impulsive phase peak that occurred at 11:57:27 UT. (a) The measured impulsive phase spectrum (black) at the time of the peak and the daily average spectrum, with flares removed, is also shown for reference (red). The absolute irradiance changes above the daily average, or the black spectrum minus the red one in (a), is shown in (b).

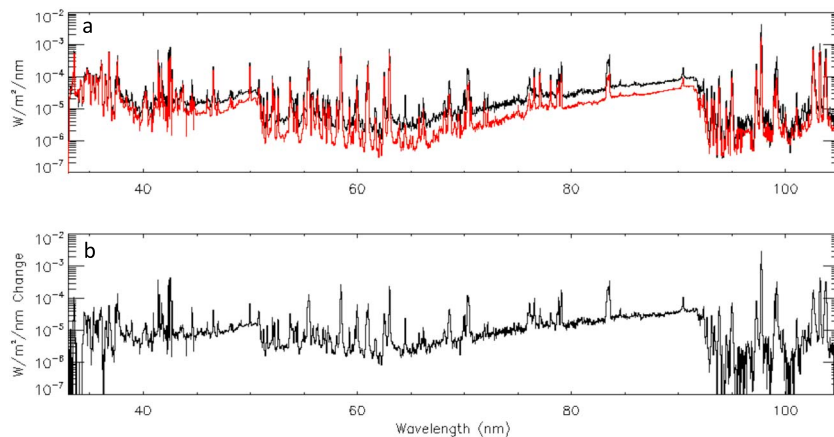


Figure 6. Spectra measured by MEGS-B during the gradual phase of the flare on 6 September 2017. A 30-s integration centered at 12:16:16 UT shows the flare spectrum (black), and the daily average spectrum (red) are shown in (a), while the absolute change of the flare over the daily average spectrum is also shown in (b). MEGS = Multiple EUV Grating Spectrograph.

timestamp in Figures 1 and 4. As seen in Figure 6, the gradual phase peak spectrum shows a larger increase at this time in the few hot coronal lines that are measured by MEGS-B, mostly the hot Fe lines in the 33–38 nm range, while the rest of the cooler emissions have decreased from their peak in the impulsive phase.

As mentioned previously, the flare-increased emissions formed in the lower solar atmosphere was occulted during the 10 September 2017 flare as viewed from Earth due to the footpoints being over-the-limb. Figure 7 shows the 30-s integration around the impulsive phase peak at 15:54:08 UT (black) and daily average (red) spectra from MEGS-B for this 10 September flare while Figure 8 shows the 30-s integration centered at the gradual phase peak at 16:07:48 UT (black) and daily average (red) spectra in the “a” panels, while the absolute changes over the daily average spectrum for that day in the “b” panels for each flare phase peak. It is a point of emphasis that the time an integration period of this impulsive phase spectrum is well before any chromospheric ribbon from subsequent reconnection along the arcade becomes visible in the AIA images around 16:05 that was mentioned earlier; therefore, this impulsive phase spectrum truly has the entire footpoints and ribbons occulted.

The spectra in Figures 7 and 8 have few significant increases in the flare spectra relative to the 10% uncertainty in MEGS-B measurements, especially for the impulsive phase spectrum in Figure 7. Larger increases

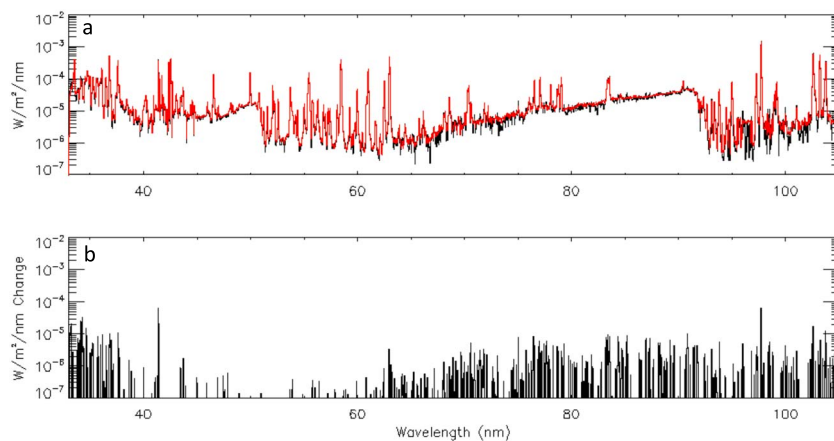


Figure 7. Spectra at the peak of the impulsive phase of the X8.2 flare on 10 September 2017 that is a 30-s integration centered at 15:54:08 UT. The flare spectrum (black) and daily average spectrum (red) are shown in (a), and the absolute change of the flare over the daily average spectrum is shown in (b). There are few significant increases seen in these spectra and most of the increases seen are simply noise.

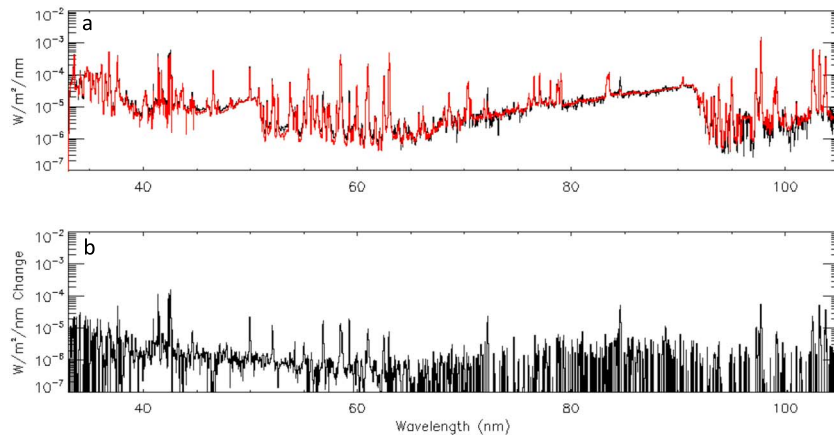


Figure 8. Thirty-second integrated gradual phase flare spectrum near the peak at 16:07:48 UT on 10 September 2017. The flare (black) and daily average (red) spectra are shown in (a), and the absolute change of the flare over the daily average spectrum is shown in (b). Many more coronal emission line increases can be seen during the gradual phase than in the impulsive phase, as expected, notably in the 33- to 38-nm emission range where some strong, hot Fe emissions exist, as well as the continuum extending to shorter wavelengths.

can be seen for known coronal emissions in Figure 8, such as the hot Fe lines that exist from 33 to 38 nm as well as the continuum extending through and to the shorter wavelengths (Milligan et al., 2012). This is expected as these hot coronal lines are formed in the coronal loops that extend above the limb of the Sun and are clearly visible from Earth as seen in Figure 2.

Given that these flares on 6 and 10 September 2017 were so similar in XRS magnitude, AIA loop and arcade evolution, and EVE time series and magnitudes, the two flares can be treated as being very similar, with the largest variable being the viewing geometry and the occulted lower atmosphere of the 10 September flare. The absolute flare spectra on 10 September given in Figure 8b, which has been shown to be from the coronal loops only, can be subtracted from the 6 September flare shown in Figure 6b, which is the entire flare including both loops and footpoints, to give an estimate of the foot point-only isolated flare emission spectra at the time of the gradual phase. This estimated foot point spectrum is shown in Figure 9, and for the most part does not look much different than the gradual flare spectrum given in Figure 6b as most of the emission in this wavelength range are cool emission from the solar atmosphere. But, there are wavelengths that extend below towards zero, meaning they are of a similar magnitude for both flares, or larger for the 10 September flare, and formed in the part of the flare that could be observed by both, the hot coronal loops. There are the aforementioned Fe emissions from 33 to 38 nm, Fe XX 56.79 nm, Fe XXI 58.58 nm and Fe XIX 59.22 nm, Fe XX 72.16 nm, and Fe XXII 84.55 nm, among others. Above 90 nm, many of the emissions going below the x-axis are due to very low signal measurements in between emission lines.

3.3. TIMED SEE Measurements

Even with TIMED SEE's 3% duty cycle, it fortuitously obtained observations very near the peak of both the 6 and 10 September flares, as well as near the peaks of the X17 flare on 28 October 2003 and the X28 flare on 4

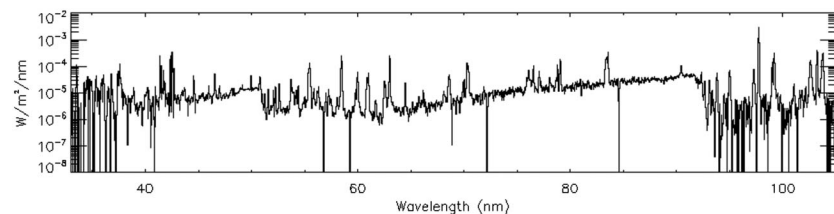


Figure 9. Difference spectrum of the 6 September flare spectrum minus the 10 September flare spectrum (e.g., spectrum in Figure 6b minus the spectrum in Figure 8b), gives an estimated spectrum of the foot point emission only, which dominates this spectral range. Dropouts are due to coronal lines, formed in the loops, that are of similar magnitude in both spectra and difference of low signal measurements above 90 nm.

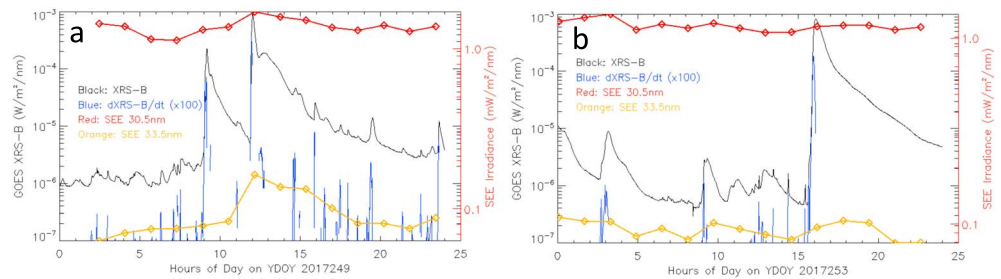


Figure 10. Time series of the 6 September (a) and 10 September (b) flares for GOES XRS (black) and dXRS/dt (blue), an indicator of the impulsive phase timing, as well as two emissions from TIMED SEE showing when the spectrograph fortuitously made its observations near the flare peak. The two emissions shown are a cool chromospheric He II emission that dominates the 30.5-nm bin (red) as well as the bin dominated by the coronal Fe XVI 33.5-nm emission line (orange). XRS = X-Ray Sensor; GOES = Geostationary Operational Environmental Satellite; TIMED = Thermosphere, Ionosphere, Mesosphere, Energetics, and Dynamics; SEE = Solar EUV Experiment.

November 2003. A time series of SEE observations for each day are shown as connected points in Figure 10, where the GOES XRS-B (black) and its time derivative (blue) are shown along with the SEE EGS relative irradiance values of the 1-nm bins centered at 30.5 nm (red), containing the He II 30.38 nm emission, and the 33.5-nm bin (green) that is dominated by the Fe XVI emission line at 33.54 nm. As seen in Figure 10, the SEE observation near the peak on 6 September was a 70-s integration starting at 12:08:12 UTC, when the GOES XRS index was below its peak (XRS is seen in black), but while it was still at Magnitude X4.9 class, and was after the impulsive phase shown as the time derivative of the GOES XRS-B, seen in blue. Significant increases in the 30.5 nm (red) bin, which is dominated by the He II emission, and 33.5 nm (green) bin, which is dominated by the Fe XVI line, can be seen at the time of this SEE flare observation. On 10 Sept, the SEE observation was another 70-s integration that started at 16:11:33 UTC when the flare index was X7.3 again just past the GOES XRS-B peak (black) but after any impulsive phase given by the blue. Even though the timing of the SEE observation is still at the time of a large increase in the GOES XRS-B, there is not a significant increase in the TIMED SEE He II 30.5-nm bin due to the occulted foot point.

The advantage of SEE is that it is a spectrograph; therefore, it measures the entire spectral range from 0 to 189 nm simultaneously. Figure 11a shows the daily average, where the average is calculated with any flare spectra removed, Version 12 SEE spectra (black) for 10 September 2017 and the flare maximum spectra for each flare, blue for the 6 September 2017 flare and red for the 10 September flare, and Figure 11b shows the ratios to the daily minimum spectrum in similar colors. Figure 11c is the irradiance difference between the 10 September flare subtracted from the 6 September flare, giving an estimate of what a spatially-resolved, flaring foot point spectrum would look like. This is similar to what was done for the EVE MEGS-B data in Figure 9, with the extended wavelength range of SEE, but with less coordinated timings due to the limited duty cycle of SEE.

It is evident in the SEE spectra and differences shown in Figure 11 that the 1-nm bins that are dominated by coronal emissions, for example, from 8 to 14 nm, for the 10 September flare have larger absolute changes than the 6 September flare. Many of the emissions show that the 10 September flare energies are significantly reduced in the cooler emissions formed in the lower solar atmosphere, such as the He II 30.4 nm emission line and the H and He free-bound continua, due to footpoints of the flare being occulted as confirmed by the significantly reduced cool emission and the images, seen later, from SDO AIA. And, as expected, these cooler emission lines from the chromosphere and transition region, along with the core of the strong H I Lyman Alpha emission line at 121.6 nm, show up and dominate the foot point spectra (panel (c)).

3.4. MAVEN EUVM Measurements

During the September 2017 storm period, the location of Mars, and therefore the MAVEN spacecraft, was approximately 15° past solar conjunction; therefore, MAVEN EUVM provided a unique vantage point and observations to study the flares. MAVEN/EUVM measured four additional flares on the backside that were not visible from Earth-based satellites such as GOES or SDO. Since both EUVM-B and GOES/XRS measure soft X-ray emissions, a scaling relationship between them can be used to estimate the GOES class of a flare from

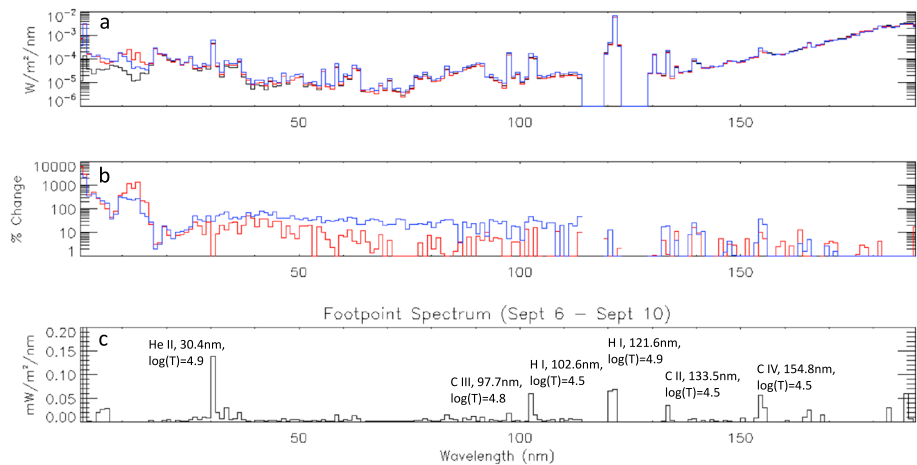


Figure 11. TIMED SEE spectra of the 6 and 10 September 2017 flares. The spectra that were taken just after the XRS peaks are shown in panel (a) for the 6 September (blue) and 10 September (red) flares, as well as the daily average spectra on 10 September 2017 (black). The spectra are measured in SEE from 27 to 190 nm at 1-nm resolution, while the results shown from 0.5 to 27 nm are the Level 4 modeled spectra at 1-nm resolution. Panel (b) shows the percent change of each flare spectra over its respective daily average spectrum. The subtraction of the 10 September spectrum from the 6 September spectrum is shown in panel (c) to give an estimation of what a spatially resolved measurement of the footpoints because the two flare spectra were of similar GOES flare class, but the 10 September flare had its footpoints occulted. The strongest emission lines, along with their formation temperature, are labeled. XRS = X-Ray Sensor; GOES = Geostationary Operational Environmental Satellite; TIMED = Thermosphere, Ionosphere, Mesosphere, Energetics, and Dynamics; SEE = Solar EUV Experiment.

EUVM. Measurements from the 0–7 nm (black) and Lyman-alpha (red) channels of EUVM for the additional flares are plotted in Figure 12, and their peak day/times, and equivalent GOES XRS class at 1 AU are given in Table 1.

A time series of this September 2017 span from the EUVM-B channel is shown in Figure 3c, but as Mars was just past solar conjunction, the flares early in this storm period were occulted from the MAVEN observation vantage point. The observed irradiance increase in EUVM between 6 and 9 September is due to the active region rotating around into view, and many of the large flares early in this storm period were completely occulted. Interestingly, the MAVEN data may be able to provide insights into energetics and timing of emissions in its three bands from observations of loop-tops of some of the early flares that had their lower profiles, including lower loops legs, occulted and only the loop-tops visible. The last flare on 10 September, where the footpoints and lower atmosphere were mostly occulted by Earth-based observatories, was fully observed by MAVEN EUVM, and is shown in Figure 13.

Chamberlin et al. (2012) has shown that flares, such as the M1.0 flare that occurred on 5 November 2010, can occur without an impulsive phase or significant increased foot point emissions. Confirmation that these cool emissions still occur in the 10 September flare comes from the EUVM instrument, where Mars was in the position to have a view of the entire flare. Figure 13 shows time series of the EUVM-B and -C channels, and

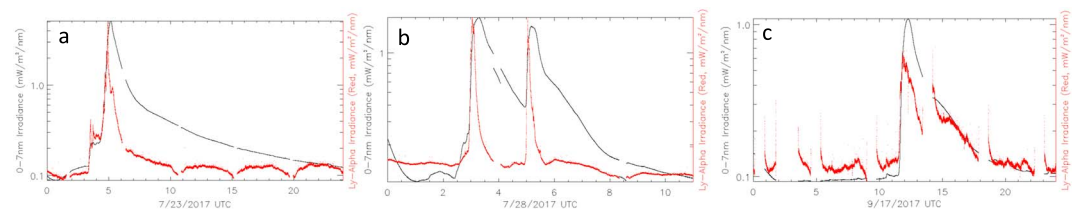


Figure 12. Time series of the MAVEN EUVM soft X-ray (0–7 nm, black) and HI Lyman-alpha (121.5 nm, red) emissions during four flares on the farside of the Sun as viewed from Earth. All flares show a strong impulsive phase in the Lyman-alpha line, an indication that these were eruptive flares. MAVEN = Mars Atmosphere and Volatile Evolution; EUVM = Extreme Ultraviolet Monitor.

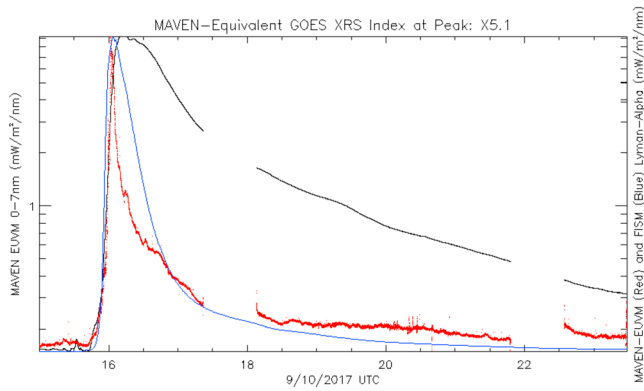


Figure 13. The MAVEN EUVM time series of the soft X-ray 0–7 nm (black) and Lyman-alpha 121.6 nm (red) emission during the 10 September flare show a very strong impulsive phase that was occulted by Earth-based measurements. The FISM2 Lyman-alpha time series (blue) is also shown for comparison. MAVEN = Mars Atmosphere and Volatile EvolutionN; EUVM = Extreme Ultraviolet Monitor.

evident is the strong increase in the Lyman-alpha channel during the impulsive phase of the flare that exhibits a “Neupert-Effect” impulsive/gradual (Lyman-alpha/soft X-ray) phase profiles (Neupert, 1968, 1989). Also shown is the FISM2 time series in blue in Figure 13, as described in the next section, whose time profile is given by the time derivative of the GOES XRS-B data. These data also show the improvement on impulsive phase timings that actual observations of Lyman-alpha, or similar chromospheric or transition region emissions, have over relying on the GOES XRS time derivative. These observations are now currently and in the foreseeable future available with GOES EUVS at Earth and with the shown EUVM-B for FISM-M. The additional EUVM measurements will help fully quantify the energetics of this flare due to the actual observations of the emission that occurred low in the solar atmosphere that are not available from any Earth-based observatory.

3.5. FISM Version 2 Model Results

The FISM2 results for the 6 September flare are presented in Figure 14. The top panel shows the daily average spectrum in black, the impulsive phase peak spectrum in red that occurred at 11:58 UT, and the gradual phase peak spectrum in blue that occurred at 12:02 UT. The middle panel shows the percent change of the impulsive (red) and gradual (blue) phase peak spectra relative to the daily average spectrum. The bottom panel shows FISM2 time series of two emissions, one the strong, cool He II emission line within the 30.35-nm bin (30.30–30.39 nm) and, because of its chromospheric source, shows a strong impulsive phase that is double peaked. The 0.1-nm bin centered at 2.05 nm is also shown. This emission is near the peak of the Bremsstrahlung continuum that is strongly enhanced during a flare thermal (gradual) phase, so it is representative of the GOES XRS and other hot coronal emissions temporal profile.

The FISM2 estimated spectrum for the 6 September 2017 flare and the TIMED SEE results (from Figure 11) are compared in Figure 15. Figure 15a shows the SEE daily average spectra (black), the SEE spectra that was measured just after the flare peak at 16:11 UT (blue), and the FISM2 estimated spectrum at the same 16:11 UT time of the SEE observation. Figure 15b shows the percent change of the SEE flare spectrum over its daily average value (black) and the FISM2 flare spectrum percent change over the FISM2 daily average spectrum for the

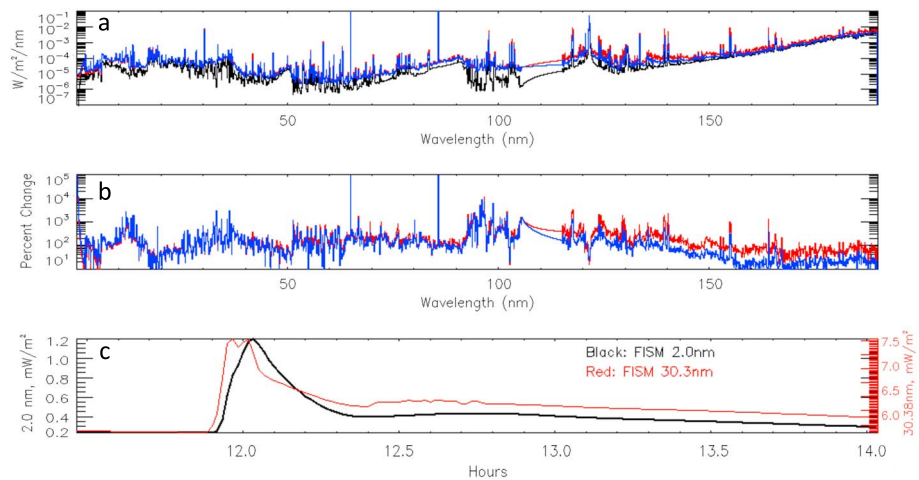


Figure 14. FISM2 estimated spectra (a), percent increase (b), and time series (c) for two emissions during the 6 September 2017 X8.9 solar flare. The spectra shown in (a) are the daily average (black), the impulsive phase peak (red, at 11:58 UT), and the gradual phase peak (blue, at 12:02 UT) spectra, while (b) shows the percent change of the gradual phase peak spectra over the daily average. Time series for two emission lines are shown in (c), the He II 30.38 nm emission of cool, chromospheric origin that is strongest during the impulsive phase, and the hot coronal emission at 2.0 nm that is near the peak of the Bremsstrahlung continuum that peaks during the gradual phase.

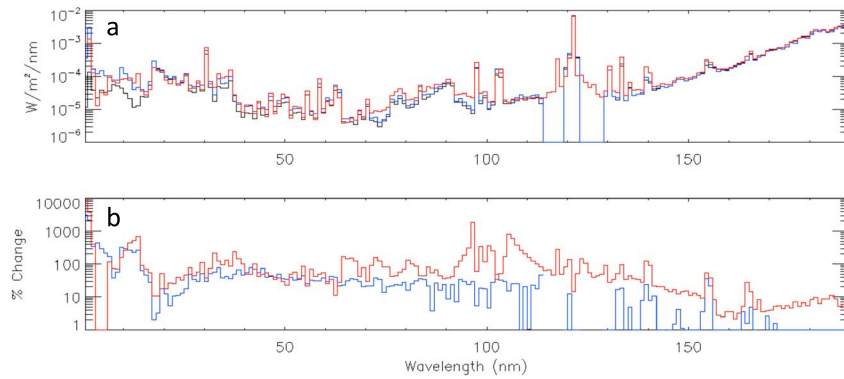


Figure 15. Panel (a) shows the comparison of the TIMED SEE daily (black) and flare (blue) measurements for the 6 September 2017 flare to the FISM2 flare estimated spectrum (red) at the same time, 16:11 UT, as the SEE flare measurement in panel (a). Panel (b) is the percent change of the SEE (blue) and FISM2 (red) flare spectra at 16:11 UT over their respective daily average spectra. TIMED = Thermosphere, Ionosphere, Mesosphere, Energetics, and Dynamics; SEE = Solar EUV Experiment.

day. All daily averages spectra are based on data sets where the daily average was computed as averages of all spectra measured for the day, but excluding ones during times of solar flares from the average so as not to bias a daily average high on those days of flares. There is good agreement at some wavelengths in the spectrum, while others need improvement. The FUV discrepancies are mostly due to the SORCE SOLSTICE being used as the base data set for FISM2 instead of TIMED SEE, and the $\sim 10\%$ difference may be largely attributed to the absolute calibration difference of the two instruments and are within the uncertainties. The other glaring difference is in the FISM2 flare results in the XUV wavelengths, where FISM2 seems to overestimate the 0- to 1-nm bin and underestimates the 4- to 6-nm bins. This is a known feature due to the SORCE XPS modeling that is planned to be improved using data from the MinXSS CubeSat (Mason et al., 2016; Woods et al., 2017), and then implemented in FISM2, in the near future to increase the accuracy of these estimations.

The FISM2 results for the 10 September flare can be produced to include the impulsive phase, as would be viewed at Mars, or to eliminate the impulsive phase component as viewed from Earth where the footpoints were occulted. The same panels as described for the 6 September flare in Figure 14 are again presented for

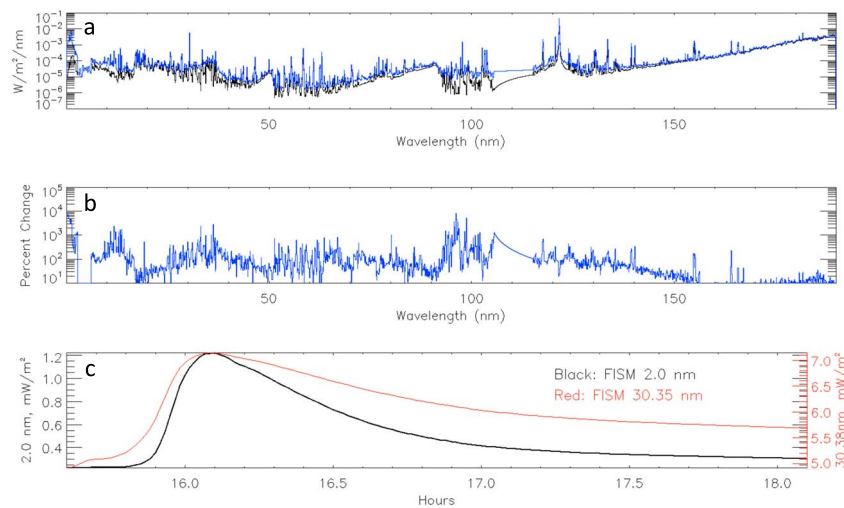


Figure 16. FISM2 estimated spectra (a), percent increase (b), and time series (c) for two emissions during the 10 September 2017 X9.3 solar flare. The spectra shown in (a) are the daily average (black) and the gradual phase peak (blue, at 16:06 UT) spectra, while (b) shows the percent change of the gradual phase peak spectra over the daily minimum. The impulsive phase (red in Figure 14a) spectrum is not shown because the footpoints were over-the-limb and occulted as viewed from Earth. Time series for two emission lines are shown in (c), the He II 30.38-nm emission of cool, chromospheric origin and the hot coronal emission at 2.0 nm that is near the peak of the Bremsstrahlung continuum.

the 10 September flare in Figure 16, but for the Earth-observation case with the impulsive phase eliminated. There is a significant reduction in the increases in the cooler emissions throughout the spectrum that are formed in the chromosphere and transition region, as these enhancements are formed in the occulted footpoints. Even though the GOES XRS class from the peak was larger and the flare duration was longer, there is overall less energy input into the Earth's ionosphere and thermosphere from this 10 September event due to the significant reduction of the cooler foot point emissions that dominate the UV wavelengths.

FISM2 data for the September 2017 events are currently available upon request from the first author, with data for other time periods available upon request until the routine FISM2 processing can be implemented and provided from the LISIRD web site where FISM1 spectra are currently available (<http://lasp.colorado.edu/lisird/>).

4. Conclusions

Studies of solar flares are limited by the amount of data available for any given event, being limited in temporal cadence, spatial resolution, and/or spectral resolution and range. Solar irradiance measurements uniquely provide important contributions due to their large spectral range and moderate spectral resolution and temporal cadence. The main advantage is that some instruments, such as SDO EVE when it was fully functional and GOES EXIS, are also able to monitor 24/7 and the entire disk, so they rarely miss a flare. The long history of these instruments allows for comparisons and statistical studies and modeling of flare events over multiple solar cycles and storm periods.

The largest solar storm of SC 24 was in September 2017, and it occurred very late in the cycle, but produced the largest flares of the entire cycle. The two largest flares on 6 and 10 September were remarkably similar in spectral irradiance profiles and physical topology. The 10 September flare was “over-the-limb” as observed from Earth and so provides unique “spatial” results of loop and foot point radiative outputs from flares, especially with the additional measurements from Mars and its unique vantage point. A key result from this study is using the one on disk and one over the limb flare to quantify and distinguish the lower flare foot point irradiance changes and upper coronal loop irradiance, with the foot point spectrum being primarily chromosphere and transition region emissions and the coronal loops being hot coronal emissions. This was qualitatively expected, but the presented solar irradiance observations in this paper can now accurately quantify the emissions from each region, foot point versus loops, throughout the UV spectral range.

Although the September 2017 flare events were well observed, there is still a need for empirical models, such as FISM2, to fill in spectral and temporal gaps in the irradiance data products. This is especially true going forward as there are no full spectral coverage replacements for MEGS-A (6–37 nm) now that it has failed, the other 21 hours a day of MEGS-B (35–105 nm), or for most of SORCE SOLSTICE (115–320 nm) that could be terminated as early as 2019. These gaps are partially covered with GOES-16 EXIS measurements of a few select emission lines in the EUV, FUV, and MUV ranges, but will more importantly be proxies for various emissions of similar temperature throughout the rest of the UV spectrum. The launch of MinXSS-2 (Woods et al., 2017) in 2018 will help cover the 0.1–2.5 nm range with high spectral resolution, but also desired is actual high-cadence, high-spectral resolution measurements to fill the spectral gap from 2.5 to 6.0 nm that is currently only modeled. This spectral range is highly variable during a solar flare and is crucial to understanding the ionospheric response to flares.

References

- Chamberlin, P. C. (2016). Measuring solar Doppler velocities in the He II 30.38 nm emission using the EUV Variability Experiment (EVE). *Solar Physics*, 291(6), 1665–1679. <https://doi.org/10.1007/s11207-016-0931-0>
- Chamberlin, P. C., Milligan, R. O., & Woods, T. N. (2012). Thermal evolution and radiative output of solar flares observed by the EUV Variability Experiment (EVE). *Solar Physics*, 279(1), 23–42. <https://doi.org/10.1007/s11207-012-9975-y>
- Chamberlin, P. C., Woods, T. N., & Eparvier, F. G. (2007). Flare Irradiance Spectral Model (FISM): Daily component algorithms and results. *Space Weather*, 5, S07005. <https://doi.org/10.1029/2007SW000316>
- Chamberlin, P. C., Woods, T. N., & Eparvier, F. G. (2008). Flare Irradiance Spectral Model (FISM): Flare component algorithms and results. *Space Weather*, 6, S05001. <https://doi.org/10.1029/2007SW000372>
- Chamberlin, P. C., Woods, T. N., Eparvier, F. G., & Jones, A. R. (2009). Next generation X-Ray Sensor (XRS) for GOES-R satellite series. *SPIE Proceedings*, 7438, 743,802–743,801. <https://doi.org/10.1117/12.826807>
- Del Zanna, G., Dere, K. P., Young, P. R., Landi, E., & Mason, H. E. (2015). CHIANTI—An atomic database for emission lines. Version 8. *Astronomy & Astrophysics*, 582, A56. <https://doi.org/10.1051/0004-6361/201526827>

Acknowledgments

P. C. C., T. N. W., and F. G. E. are supported by the SDO/EVE project at CU/LASP (PI Tom Woods). P. C. C., E. M. B. T., and F. G. E. are NASA Living with a Star grant NNX16AE86G titled, “Improving Solar EUV Spectral Irradiance Models with Multi-Vantage Point Observations” (PI Frank Eparvier), and the NASA MAVEN Project (PI Bruce Jakosky). P. C. C. would like to thank the anonymous reviewers that greatly improved this manuscript with their detailed comments and suggestions. The data used are listed in the references. This study used the CHIANTI database; CHIANTI is a collaborative project involving George Mason University, the University of Michigan (USA), and the University of Cambridge (UK). The team also would like to acknowledge the Heliviewer.org teams and NASA, ESA, and NOAA for their support of this study with their publicly available data and analysis tools. Sunspot data are from the WDC-SILSO, Royal Observatory of Belgium, Brussels. The FISM2 data used here are now publicly available on the LISIRD data site on the FISM page, or directly here: http://lasp.colorado.edu/lisird/resources/lasp/fism2/FISM2_Sept_2017_Storm.zip.

- Dere, K. P., Landi, E., Mason, H. E., Monsignor Fossi, B. C., & Young, P. R. (1997). CHIANTI—An atomic database for emission lines. *Astronomy & Astrophysics, Supplement Series*, 125(1), 149–173. <https://doi.org/10.1051/aas:1997368>
- Didkovsky, L., Judge, D., Wieman, S., Woods, T., & Jones, A. (2012). EUV SpectroPhotometer (ESP) in extreme ultraviolet variability experiment (EVE): Algorithms and calibrations. *Solar Physics*, 275(1–2), 179–205. <https://doi.org/10.1007/s11207-009-9485-8>
- Eparvier, F. G., Chamberlin, P. C., Woods, T. N., & Thiemann, E. M. B. (2015). The solar extreme ultraviolet monitor for MAVEN. *Space Science Reviews*, 195(1–4), 293–301. <https://doi.org/10.1007/s11214-015-0195-2>
- Eparvier, F. G., Crotser, D., Jones, A. R., McClintock, W. E., Snow, M., & Woods, T. N. (2009). The Extreme Ultraviolet Sensor (EUVS) for GOES-R. *SPIE Proceedings*, 7438, 743804. <https://doi.org/10.1117/12.826445>
- García, H. A. (1994). Temperature and emission measure from GOES soft X-ray measurements. *Solar Physics*, 154(2), 275–308. <https://doi.org/10.1007/BF00681100>
- Hock, R. A., Woodraska, D., & Woods, T. N. (2013). Using SDO EVE data as a proxy for GOES XRS B 1–8 angstroms. *Space Weather*, 11, 262–271. <https://doi.org/10.1002/swe.20042>
- Hudson, H. S., Woods, T. N., Chamberlin, P. C., Fletcher, L., Del Zanna, G., Didkovsky, L., et al. (2011). The EVE Doppler sensitivity and flare observations. *Solar Physics*, 273(1), 69–80. <https://doi.org/10.1007/s11207-011-9862-y>
- Jakosky, B. M., Lin, R. P., Grebowsky, J. M., Luhmann, J. G., Mitchell, D. F., Beutelschies, G., et al. (2015). The Mars Atmosphere and Volatile Evolution (MAVEN) mission. *Space Science Reviews*, 195(1–4), 3–48. <https://doi.org/10.1007/s11214-015-0139-x>
- Kopp, G., Lawrence, G., & Rottman, G. (2005). The Total Irradiance Monitor (TIM): Science results. *Solar Physics*, 230(1–2), 129–139. <https://doi.org/10.1007/s11207-005-7433-9>
- Landi, E., Young, P. R., Dere, K. P., Del Zanna, G., & Mason, H. E. (2013). CHIANTI—An atomic database for emission lines. XIII. Soft X-ray improvements and other changes. *The Astrophysical Journal*, 763(2), 86. <https://doi.org/10.1088/0004-637X/763/2/86>
- Lemen, J. R., Akin, D. J., Boerner, P. F., Chou, C., Drake, J. F., Duncan, D. W., et al. (2012). The atmospheric imaging assembly (AIA) on the Solar Dynamics Observatory (SDO). In P. Chamberlin, W. D. Pesnell, & B. Thompson (Eds.), *The Solar Dynamics Observatory* (pp. 17–40). US: Springer.
- Lolo, A., Withers, P., Fallows, K., Girazian, Z., Matta, M., & Chamberlin, P. C. (2012). Numerical simulations of the ionosphere of Mars during a solar flare. *Journal of Geophysical Research*, 117, A05314. <https://doi.org/10.1029/2011JA017399>
- Mason, J. P., Woods, T. N., Caspi, A., Chamberlin, P. C., Moore, C., Jones, A., et al. (2016). Miniature X-ray solar spectrometer: A science-oriented, University 3U CubeSat. *Journal of Spacecraft and Rockets*, 53(2), 328–339. <https://doi.org/10.2514/1.A33351>
- McClintock, W. E., Rottman, G. J., & Woods, T. N. (2005). Solar-Stellar Irradiance Comparison Experiment II (Solstice II): Instrument concept and design. *Solar Physics*, 230(1–2), 225–258. <https://doi.org/10.1007/s11207-005-7432-x>
- Milligan, R. O., Chamberlin, P. C., Hudson, H. S., Woods, T. N., Mathioudakis, M., Fletcher, L., et al. (2012). Observations of enhanced extreme ultraviolet continua during an X-class solar flare using SDO/EVE. *The Astrophysical Journal*, 748(1), L14. <https://doi.org/10.1088/2041-8205/748/1/L14>
- Milligan, R. O., Kerr, G. S., Dennis, B. R., Hudson, H. S., Fletcher, L., Allred, J. C., et al. (2014). The radiated energy budget of chromospheric plasma in a major solar flare deduced from multi-wavelength observations. *The Astrophysical Journal*, 793(2), 70. <https://doi.org/10.1088/0004-637X/793/2/70>
- Moore, C. S., Chamberlin, P. C., & Hock, R. (2014). Measurements and modeling of total solar irradiance in X-class solar flares. *The Astrophysical Journal*, 787(1), 32. <https://doi.org/10.1088/0004-637X/787/1/32>
- Neupert, W. M. (1968). Comparison of solar X-ray line emission with microwave emission during flares. *The Astrophysical Journal*, 153, L59. <https://doi.org/10.1086/180220>
- Neupert, W. M. (1989). Transient coronal extreme ultraviolet emission before and during the impulsive phase of a solar flare. *The Astrophysical Journal*, 344, 504–512. <https://doi.org/10.1086/167819>
- Pesnell, W. D., Thompson, B. J., & Chamberlin, P. C. (2012). The Solar Dynamics Observatory (SDO). *Solar Physics*, 275(1–2), 3–15. <https://doi.org/10.1007/s11207-011-9841-3>
- Peterson, W. K., Chamberlin, P. C., Woods, T. N., & Richards, P. G. (2008). Temporal and spectral variations of the photoelectron flux and solar irradiance during an X class solar flare. *Geophysical Research Letters*, 35, L12102. <https://doi.org/10.1029/2008GL033746>
- Qian, L., Burns, A. G., Chamberlin, P. C., & Solomon, S. C. (2010). Flare location on the solar disk: Modeling the thermosphere and ionosphere response. *Journal of Geophysical Research*, 115, A09311. <https://doi.org/10.1029/2009JA015225>
- Qian, L., Burns, A. G., Chamberlin, P. C., & Solomon, S. C. (2011). Variability of the thermosphere and ionosphere response to solar flares. *Journal of Geophysical Research*, 116, A10309. <https://doi.org/10.1029/2011JA016777>
- Qian, L., Burns, A. G., Liu, H., & Chamberlin, P. C. (2012). Solar flare impacts on ionospheric electrodynamics. *Geophysical Research Letters*, 39, L06101. <https://doi.org/10.1029/2012GL051102>
- Qian, L., Burns, A. G., Solomon, S. C., & Chamberlin, P. C. (2012). Effect of a solar flare on a traveling atmospheric disturbance. *Journal of Geophysical Research*, 117, A10319. <https://doi.org/10.1029/2012JA017806>
- Rottman, G. (2005). The SORCE Mission. *Solar Physics*, 230(1–2), 7–25. <https://doi.org/10.1007/s11207-005-8112-6>
- Ryan, D. F., Chamberlin, P. C., Milligan, R. O., & Gallagher, P. T. (2013). Decay-phase cooling and inferred heating of M- and X-class solar flares. *The Astrophysical Journal*, 778(1), 68. <https://doi.org/10.1088/0004-637X/778/1/68>
- Snow, M., McClintock, W. E., Crotser, D., & Eparvier, F. G. (2009). EUVS-C: The measurement of the magnesium II index for GOES-R EXIS. *Proceedings of SPIE*, 7438, 743803. <https://doi.org/10.1117/12.828566>
- Sternovsky, Z., Chamberlin, P., Horanyi, M., Robertson, S., & Wang, X. (2008). Variability of the lunar photoelectron sheath and dust mobility due to solar activity. *Journal of Geophysical Research*, 113, A10104. <https://doi.org/10.1029/2008JA013487>
- Thieman, E. M. B., Chamberlin, P. C., Eparvier, F. G., & Epp, L. (2018). Center-to-limb variability of hot coronal EUV emissions during solar flares. *Solar Physics*, 293(2), 19. <https://doi.org/10.1007/s11207-018-1244-2>
- Thieman, E. M. B., Chamberlin, P. C., Eparvier, F. G., Templeman, B., Woods, T. N., & Bougher, S. W. (2017). The MAVEN EUVM model of solar spectral irradiance variability at Mars: Algorithms and results. *Journal of Geophysical Research: Space Physics*, 122, 2748–2767. <https://doi.org/10.1002/2016JA023512>
- Woods, T. N., Caspi, A., Chamberlin, P. C., Jones, A., Kohnert, R., Mason, J. P., et al. (2017). New solar irradiance measurements from the miniature X-ray solar spectrometer CubeSat. *The Astrophysical Journal*, 835(2), 122. <https://doi.org/10.3847/1538-4357/835/2/122>
- Woods, T. N., Chamberlin, P. C., Peterson, W. K., Meier, R. R., Richards, P. G., Strickland, D. J., et al. (2008). XUV photometer system (XPS): Improved irradiance algorithm using CHIANTI spectral models. *Solar Physics*, 249. <https://doi.org/10.1007/s11207-008-9196-6>
- Woods, T. N., Eparvier, F. G., Bailey, S. M., Chamberlin, P. C., Lean, J., Rottman, G. J., et al. (2005). The Solar EUV Experiment (SEE): Mission overview and first results. *Journal of Geophysical Research*, 110, A01312. <https://doi.org/10.1029/2004JA010765>

- Woods, T. N., Eparvier, F. G., Hock, R., Jones, A. R., Woodraska, D., Judge, D., et al. (2012). Extreme Ultraviolet Variability Experiment (EVE) on the Solar Dynamics Observatory (SDO): Overview of science objectives, instrument design, data products, and model developments. *Solar Physics*, 275(1–2), 115–143. <https://doi.org/10.1007/s11207-009-9487-6>
- Woods, T. N., Hock, R., Eparvier, F., Jones, A. R., Chamberlin, P. C., Klimchuk, J. A., et al. (2011). New solar extreme- ultraviolet irradiance observations during flares. *The Astrophysical Journal*, 739(2), 59. <https://doi.org/10.1088/0004-637X/739/2/59>
- Woods, T. N., Kopp, G., & Chamberlin, P. C. (2006). Contributions of the solar ultraviolet irradiance to the total solar irradiance during large flares. *Journal of Geophysical Research*, 111, A10S14. <https://doi.org/10.1029/2005JA011507>
- Woods, T. N., & Rottman, G. (2005). XUV Photometer System (XPS): Solar variations during the SORCE Mission. *Solar Physics*, 230(1-2), 375–387. <https://doi.org/10.1007/s11207-005-2555-7>
- Yang, S., Zhang, J., Zhu, X., & Qiao, S. (2017). Block-induced complex structures building the flare-productive Solar Active Region 12673. *The Astrophysical Journal Letters*, 849(2), L21. <https://doi.org/10.3847/2041-8213/aa9476>